On the Czochralski growth of Si_xGe_{1-x} crystals as substrates for strained Ge quantum well heterostructures

Aravind N. Subramanian ; Carsten Richter ; Alexander Gybin; Merve P. Kabukcuoglu ; Elias Hamann ;
Marcus Zuber ; Maximilian Oezkent ; Christo Guguschev ; Uta Juda ; Thomas Schroeder ;
Nikolay V. Abrosimov ; R. Radhakrishnan Sumathi ; Kevin-P. Gradwohl

Check for updates

View Online Export Citation

Articles You May Be Interested In

Thermal conductivity of nanostructured Si_xGe_{1-x} in amorphous limit by molecular dynamics simulation

J. Appl. Phys. (June 2015)

Effect of compressive and tensile strain on misfit dislocation injection in SiGe epitaxial layers

J. Vac. Sci. Technol. B (May 1993)

High-speed GaAs metal gate semiconductor field effect transistor structure grown on a composite Ge∕Ge x Si 1 − x∕Si substrate

J. Appl. Phys. (April 2007)

AIP Publishing

On the Czochralski growth of Si$_x$Ge$_{1-x}$ crystals as substrates for strained Ge quantum well heterostructures

View Online   Export Citation   CrossMark

Aravind N. Subramanian,[1] Carsten Richter,[1] Alexander Gybin,[1] Merve P. Kabukcuoglu,[2] Elias Hamann,[2] Marcus Zuber,[2] Maximilian Oezkent,[1] Christo Guguschev,[1] Uta Juda,[1] Thomas Schroeder,[1,3] Nikolay V. Abrosimov,[1] R. Radhakrishnan Sumathi,[1] and Kevin-P. Gradwohl[1,a)]

AFFILIATIONS

[1]Leibniz-Institut für Kristallzüchtung, Max-Born-Straße 2, Berlin 12489, Germany
[2]Institute for Photon Science and Synchrotron Radiation (IPS), Karlsruhe Institute of Technology (KIT), Hermann-von-Helmholtz-Platz 1, Eggenstein-Leopoldshafen 76344, Germany
[3]Institut für Physik, Newtonstr. 15, Humboldt-Universität Berlin, Berlin, Germany

[a)]Author to whom correspondence should be addressed: kevin-peter.gradwohl@ikz-berlin.de

ABSTRACT

This investigation showcases the viability of producing Si$_x$Ge$_{1-x}$ bulk single crystals via the Czochralski technique. A high Si content in Ge-rich SiGe wafers is highly desirable for various applications in quantum technology, particularly as strain-relaxed buffers for the realization of hole spin qubits in strained Ge quantum well heterostructures. The focus lies on the bulk crystal growth of such materials and their chemical and structural quality. For this, the Czochralski process, starting from a highly pure Ge seed and melt, utilizing continuous feeding by dissolution of Si rods was performed. Si$_{0.16}$Ge$_{0.86}$ wafers with a diameter of up to 15 mm obtained from the bulk crystal exhibited homogeneous structural quality in contrast to the conventionally used epitaxial strain-relaxed SiGe buffers. The compositional fluctuations of Si measured throughout the wafer were below 0.4 at. % in addition to a dislocation density below 3×10^6 dislocations/cm^2. Interestingly, the central region of the wafer displayed no measurable compositional fluctuations and contained less than 10^5 dislocations/cm^2. Furthermore, the difficulties and limits of growing such SiGe crystals are discussed, such as the continuous dissolution of Si during growth and the formation of oxides in the melt during growth. The current observations indicate significant potential for further enhancement of the crystal quality and to realize higher Si concentrations using the Czochralski technique.

INTRODUCTION

Quantum computing platforms based on spin qubits achieved in gate-defined quantum dots (QDs) realized in strained group IV semiconductor single-crystal layers have emerged as a prominent candidate because of their scalability. Compressively strained Ge quantum well (QW) heterostructures on SiGe (i.e., Ge/SiGe) are one of the leading material platforms for hole spin qubit technology primarily attributed to the low effective mass of holes in Ge, a low noise qubit environment, and an impressive control over the QDs.[1,2] Furthermore, the strained Ge QWs enable the realization of heavy-hole (HH) qubits, which operate at T > 1 K,[2] thus simplifying the demanding circuit

requirements. Over the last year, several crucial achievements have been reported, which include single-hole spin qubit control,[3] four-qubit quantum processor,[4] realizing hopping spin-based logic[5] as well as scalable 16 quantum dot systems.[6] However, quantum decoherence limits the operation of larger systems, and while Ge and Si can be isotopically enriched to reduce decoherence by hyperfine interaction, the material perfection of SiGe virtual substrates will limit the further improvement of the technology.[7] This includes but is not limited to (1) electrically active impurities causing charge noise, (2) compositional inhomogeneity in these layers causing strain fluctuations, and (3) high density of threading dislocations.

04 March 2025 09:07:20

Currently, the state-of-the-art Ge quantum wells in Ge/SiGe heterostructures utilize epitaxially grown Si_xGe_{1-x} strain-relaxed buffers ($x\sim0.2$) on Si substrates. Consequently, epitaxy from the Si wafer can be directly forward-graded to Ge-rich SiGe buffers or reverse-graded from a thick strain-relaxed Ge virtual substrate on Ge or Si. These Ge-rich SiGe substrates typically exhibit threading dislocation densities (TDDs) ranging from 10^6 to 10^7 cm^{-2} due to the large lattice mismatch with pure Si. Recently, an advancement was made by directly forward-grading Ge-rich SiGe buffers from Ge substrates, which reduced threading dislocation densities down to 6×10^5 cm^{-2}. These buffers also exhibited a low percolation density, high mobility of quantum wells, and low noise quantum dot qubits,[8] thereby promising a high performance of the spin qubits.[7] However, fundamentally, all graded SiGe buffer approaches will inherently exhibit non-negligible TDD.[9] Additionally, due to the dislocation-mediated strain relaxation mechanism accompanied by an inhomogeneous strain distribution, the buffer layer will suffer from compositional undulations, referred to as the cross-hatch pattern.[10–12]

The Czochralski (Cz) method is one of the most important techniques for producing large diameter bulk single crystals with very low dislocation densities of a wide variety of electronic and optical materials. This study demonstrates the potential of Ge-rich SiGe bulk crystals, grown from melt by the Cz method, to fabricate substrates for the Ge-based heterostructures, thereby improving the promising material platform for quantum computing (see Fig. 1). The substrates obtained from the bulk single $Si_{0.2}Ge_{0.8}$ crystals

instead of the conventionally used strain-relaxed buffers can induce the required heteroepitaxial strain required to produce a quantum well. The optimization of the Dash necking procedure and other growth parameters during the Cz growth could potentially facilitate the growth of dislocation-free crystals,[13] without compositional fluctuations thereby avoiding the cross-hatch pattern. While alternative approaches, such as using nanomembrane platforms like GaAs, facilitate the fabrication of low dislocation Ge-rich SiGe single crystalline layers with thicknesses limited to a few nanometers,[14] the Cz method produces crystals with a superior chemical purity, a parameter of critical importance for qubit technology. Additionally, substrates obtained from bulk crystals would decrease the hetero-epitaxial steps required to produce the heterostructure.

The single-crystal bulk growth of Ge-rich Si_xGe_{1-x} particularly, with high Si concentration, is very challenging due to the large difference between the equilibrium concentrations of Si in the Ge melt and crystal at a given temperature. Hence, the transport of Si from the melt to the crystal is crucial. Additionally, as the Si concentration in the melt varies, the melting point varies, leading to, e.g., constitutional supercooling at the crystal–melt interfaces, thus resulting in polycrystalline growth. Inhomogeneous mixing of the Si_xGe_{1-x} melt can result in the formation of a dendrite network at Si-rich regions, impeding the crystal growth experiment. To date, the highest reported Si concentration in Si_xGe_{1-x} single crystals has been limited to $x = 0.15$.[15–17] However, the aforementioned advantages strongly motivate further investigation into bulk crystal growth research for obtaining homogeneous SiGe substrates (see Fig. 1).

EXPERIMENTAL DESCRIPTION

Crystal growth

The Si_xGe_{1-x} bulk single crystal investigated in this work was grown using the Czochralski method with continuous feeding of Si as shown in Fig. 2. The process begins by melting the feed material

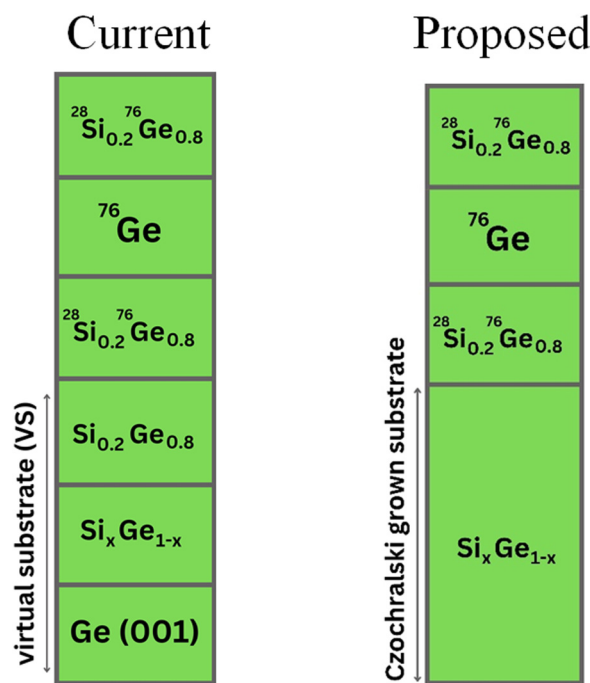FIG. 1. Schematic of the $Ge_{1-x}Si_x$-based current heterostructure utilizing strain-relaxed SiGe buffer layers and the proposed heterostructure on Cz-SiGe for Ge-based hole-spin qubits.
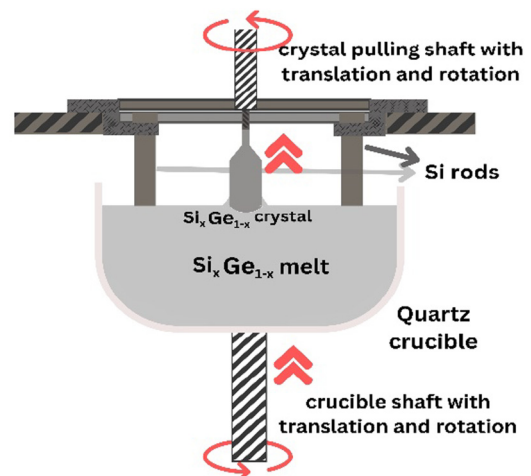

FIG. 2. Schematic of the crystal growth setup to grow SiGe single crystals using continuous feeding of Si by Si rods.[15]

04 March 2025 09:07:20

in a suitable crucible, using either a resistance or an induction heater. Subsequently, a seed (typically a single crystal of the same material with surfaces cut at a specific crystallographic orientation) is lowered and dipped into the free surface of the melt. Upon reaching an equilibrium, a meniscus forms at the interface between the seed and the melt. As the seed is gradually pulled upward, crystallization occurs at the interface, thus resulting in the formation of a new single crystalline volume. In this work, 750 g of electronic-grade polycrystalline Ge feed with a resistivity of 50 Ωcm (net charge carrier density of $\sim 10^{13}$ cm^{-3}) was melted in a quartz crucible utilizing a graphite resistance heater. The crystal growth was initiated using a [100] Ge seed crystal, which was dipped into a pure Ge melt followed by the gradual introduction of Si into the Ge melt. Furthermore, the crucible and the crystal were rotated in opposite directions to achieve better melt convection leading to better mixing, thus reducing the thickness of the boundary layer on the solid–liquid interface. Following the formation of the crystal neck, the crucible was vertically translated upward, facilitating contact between the Si rods and the Ge melt. The Si concentration in the Ge melt was regulated by controlling the volume of the Si rods submerged in the melt. For this, six Si rods were securely positioned on the stationary frame above the crucible, ensuring sixfold symmetrical placement around the growing crystal. The furnace design used in this work was inspired by the setup reported by Abrosimov et al.[15] This arrangement is critical, as any asymmetry surrounding the growing crystal within the melt could induce an uneven temperature distribution, leading to the initiation of parasitic nucleation sources.[15,18] The upward translation was carried out gradually, with a speed of 0.5 mm/h. The crucible was translated for a duration of 55 h, consequently immersing approximately 22.5 mm of Si rods in the melt. The pulling shaft/rod was translated at a rate of 1.5 mm/h, resulting in a net crystal growth rate of around 1.0 mm/h. Furthermore, the increase in the Si concentration in the melt was accompanied by an adequate increase in the heater power. Notably, at temperatures close to the crystallization point of Ge (938 °C), the dissolution of Si into the Ge melt occurs at an extremely slow rate due to the low solubility of Si in Ge at these temperatures. Consequently, any temperature increments within the system must be carefully controlled to minimize potential adverse effects on the growing crystal. Prior to growth, the Si rods and the Ge feed material underwent wet-chemical etching using a solution of HF (40 wt. %):HNO$_3$(65 wt. %) mixed in a 3:1 volume ratio for a duration of 3 min and rinsed using de-ionized water The grown crystal amounted to approximately 5% of the total melt in the crucible. The crystal growth was carried out in an Ar atmosphere (6 N) with a flow rate of up to 10 Nl/min.

Material characterization

X-ray fluorescence mapping

The Si concentration in the crystal was determined by micro x-ray fluorescence (μ-XRF) spectroscopy utilizing a BRUKER M4 TORNADO spectrometer. The measurement system was equipped with a rhodium x-ray source operated at 50 kV and 200 μA for point measurements and at 50 kV and 200 μA for the element distribution maps. Poly-capillary x-ray optics were used to focus the

non-polarized white radiation at the surface of the sample, resulting in a spatial resolution of about 20 μm.

The point measurements were performed on polished samples obtained from the crystal under low vacuum conditions (20 mbar), and the spectra were recorded for each measured point for 100 s. For determination of the chemical composition, the spectrometer was fine-calibrated using a standard section of the grown crystal that had been measured by x-ray diffraction (see below in the next paragraph) to avoid an underestimation of the Si content in the samples, due to the partial absorption of the Si fluorescence in the Ge-rich matrix when using the standard-free fundamental parameter approach based on Sherman's equation.[19] The composition of the standard reference section was calculated from lattice parameter data obtained by x-ray diffraction (see below in the next paragraph).

For the elemental mapping, the measurement time per point was set to 20 ms and all spots were measured four times to increase the counting statistics, i.e., four passes of the scans were performed. The step distance between the individual points was 19 μm. On the same tool, energy-dispersive Laue mapping (EDLM)[20] was conducted under similar measurement conditions at 200–600 μA (3–4 cycles, step distance: 12–20 μm, 20 ms measurement time per point) to identify small-angle grain boundaries and striations present in the crystal.

Rocking curve imaging

The lattice parameter and the consequent Si concentration were mapped on a wafer scale utilizing x-ray diffraction rocking curve imaging (RCI), which was developed previously using a Rigaku SmartLab diffractometer.[21] The setup included a copper (Cu) anode as the x-ray source (Cu-Kα_1 radiation, $\lambda = 1.540\,562$) and a Ge 400 double-crystal monochromator. Here, RCI measurements were performed for each of the 224 reflections from an (001) oriented wafer involving rotations about the surface normal by $\varphi = 0°, 90°, 180°$, and $270°$. The HyPix-30002D pixel detector was used to obtain angular resolution in the scattering plane as well as a spatial resolution of 200 μm perpendicular to the scattering plane. The latter was enabled by adding a parallel slit analyzer with an angular acceptance of 0.114° in front of the detector. By additionally scanning the sample through the line-shaped x-ray beam with dimensions of 0.2 × 8 mm (parallel and perpendicular to the scattering plane), a 4D RCI map comprising the two spatial surface dimensions and, for each point, 2D reciprocal space maps of diffraction intensity near the corresponding 224 Bragg peak was obtained. The obtained positions of the reciprocal lattice vectors $\mathbf{G}_{224}$, $\mathbf{G}_{2\bar{2}4}$, $\mathbf{G}_{\bar{2}24}$, and $\mathbf{G}_{\bar{2}\bar{2}4}$ are linearly combined to determine the unit-cell basis vectors for the reciprocal and, subsequently, the direct lattice. From the latter, the unit-cell volume V_{uc} that is related to the Si-concentration x in Si$_x$Ge$_{1-x}$ was computed using $\sqrt[3]{V_{uc}(x)} = a_0(x) = 5.431\,\text{Å} + 0.20\,\text{Å}x + 0.027\,\text{Å}x^2$.[22]

White-beam x-ray topography

White-beam synchrotron x-ray topography (WB-XRT) measurements were performed at the topography station of the Imaging cluster of the Karlsruhe Institute of Technology (KIT) light source.[23] The topography images on selected reflections were recorded using a 2D x-ray detector consisting of a 200 μm thick LuAG:Ce
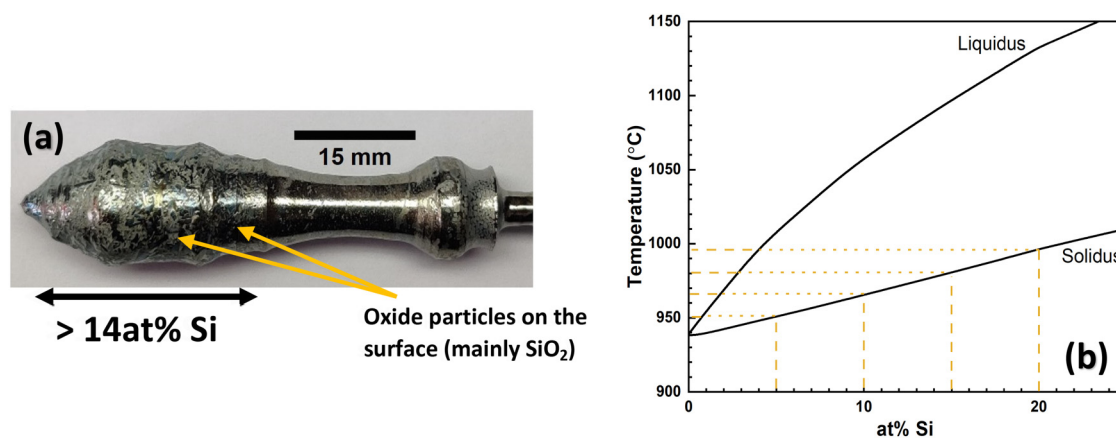
<div style="text-align: right">04 March 2025 09:07:20</div>

FIG. 3. (a) Grown Si_xGe_{1-x} crystal with the marked region containing more than 14 at. % Si and (b) equilibrium phase diagram of the Ge-rich Si–Ge system up to 30 at. % Si (adapted from Ref. 25).

scintillator crystal coupled to a CCD camera (pco.4000 with 4008×2672 pixels) with $2.5\,\mu m$ effective pixel size. The x-ray beam size was set to approximately $7 \times 4.5\,mm^2$. The sample was measured in transmission geometry on a (100) longitudinal cut cross section of the crystal. For recording the 040 reflection, the sample was accordingly tilted to a Bragg angle of 8.7° and the detector was set with a tilt angle of 15°. The beam exposure time was 5 s.

Etch pit density (EPD) analysis

The dislocation density was analyzed using wet-chemical defect-selective etching. The samples were etched using preferential etchants revealing the dislocations terminating at the surface of the sample. For this, the SECCO etch was employed (HF:0.15 m $K_2Cr_2O_7$ solution = 2:1) with an etch time of 45 s, a standard procedure for dislocation-selective etching of SiGe.[24] The resulting etch pits were analyzed and counted using optical microscopy utilizing differential interference contrast.

QUANTITATIVE ANALYSIS OF THE PROPERTIES OF THE GROWN Si_xGe_{1-x} CRYSTAL

A photograph of the grown single crystalline Si_xGe_{1-x} crystal is shown in Fig. 3(a). The maximum diameter was about 15 mm, and the Si concentrations measured in this region were around 18 at. %. The observed discontinuities in crystal diameter are attributed to the continuous, increase in Si concentration during the growth process and the associated increase in crystallization temperature [Fig. 3(b)]. Hence, maintaining stable crystallization conditions at the melt–crystal interface is challenging and can only be achieved by continuous adjustment and, in general, a gradual increment of the growth temperature.

Despite etching the source materials, Si feed rods, and conducting the growth process in an inert/controlled atmosphere, the formation of oxide particles floating on the melt surface over the long growth duration of days was observed. Several oxide particles floating on the melt surface adhered to the outer surface of the crystal as

can be seen in Fig. 3(a). Preventing the formation of oxides (e.g., by using reduced growth atmospheres) and achieving a homogeneous dissolution of Si in the Ge melt are critical to improving the crystal quality. Furthermore, the oxides could potentially serve as additional nucleation sources and adversely affect the growth experiment.

Toward the end of the growth experiment, approximately 13.4 g of Si was dissolved in the Ge melt, which corresponds to 3.4 at. % Si in the Ge melt. This corresponds to a Si concentration of approximately 19 at. % in the crystal in thermodynamic equilibrium. For further analysis, (0 0 1) wafers perpendicular to the growth direction (~16.5 at. % Si) and a (011) wafer parallel to the growth (1 at. %–16 at. % Si) direction were cut from the crystal. The wafers were chemo-mechanically polished (CMP) to an RMS roughness below 1 nm.

Si incorporation in the crystal

The Si concentration throughout the crystal was determined by μ-XRF. The Si concentration profile along the crystal is depicted in Fig. 4(a). The Si concentration gradually increases from 0% in the top region of the crystal to 16%–19% in the constant diameter body and goes close to 20% toward the tail end. The XRF map of the crystal cross section is shown in Fig. 4(b). The XRF map reveals distinct regions separated by abrupt increases in Si incorporated in the crystal volume. Additionally, these Si concentration "jumps" are observed to be discontinuous along the crystal length. Given the large segregation coefficient of Si in Ge, these "jumps" may be attributed to the irregular dissolution of Si from the rods into the Ge melt. Although the precise reason remains to be investigated, several factors could influence the Si dissolution in the Ge melt, including inhomogeneous mixing resulting in Si-rich "rings" around each Si rod, the system's heat and melt flow characteristics, and the oxidation of the surface of the Si rods during the growth experiment.[15,26,27]

The concentration of electrically active impurities in the SiGe crystal was determined by resistivity measurements along the [001] growth direction of the crystal using the four-point probe method.
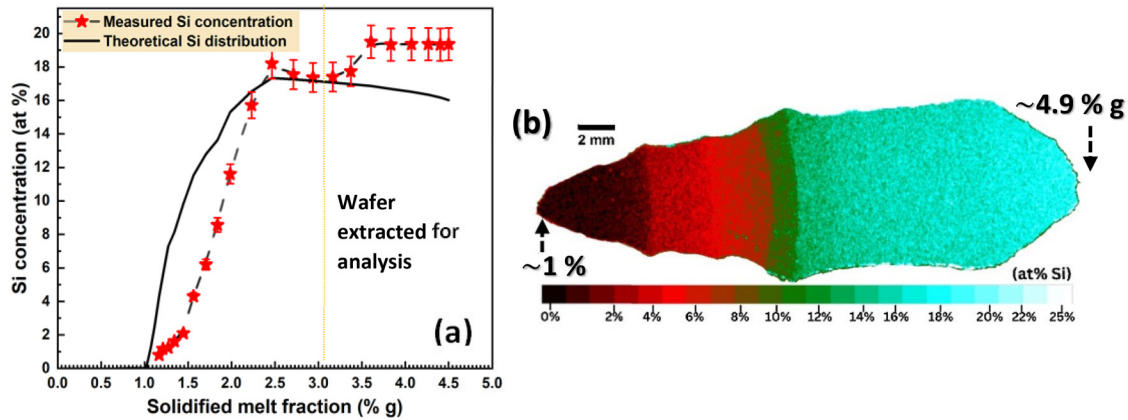
04 March 2025 09:07:20

FIG. 4. (a) Si distribution in the grown crystal measured using the μ-XRF technique along the percentage solidified melt fraction (% g) compared to the theoretical segregation of Si calculated using the Scheil equation. (b) XRF map of the crystal depicting the measured Si distribution.

The resistivity increased from 40 Ohm cm in the pure Ge part (up to 1% g) to approximately 600 Ohm cm toward the tail end (5% g). The increase in resistivity toward the tail end can ascribed to the drop in carrier mobility with increasing Si incorporation.[28] The high resistivity throughout the crystal suggests that no major amount of electrically active impurities was introduced during growth, and the crystal contains a net charge carrier density of the starting material of $\sim 10^{13}\,\text{cm}^{-3}$, which is better than purities achieved in even the purest epitaxy reactors and processes.

The theoretical segregation of Si in the solidified melt fraction (g) was obtained by considering the continuous dissolution of Si from the rods into the melt. The calculated Si profile was compared to the measured μ-XRF concentration and is shown in Fig. 4(a). For the calculation, instantaneous dissolution of the Si rods in the Ge melt upon contact was assumed. Furthermore, the corresponding $\text{Si}_x\text{Ge}_{1-x}$ melt was assumed to be homogeneous. Considering the large difference in the volume of the solidifying melt fraction and the total melt volume, the incorporation of Si in the growing crystal has a negligible reduction effect on the total Si concentration in the melt. Thereby, the concentration of Si in the melt as a function of time while translating the crucible upwards (C_0) is given by

$$[C_0]_t = \sum_{t=0}^{t_m} [(1.88 \times 10^{22}) \times [(w_{Si})_t],$$

where 1.88×10^{22} is the conversion factor, w_{Si} is the weight of Si dissolved in the Ge melt, "t" represents the time elapsed after initiating the upward translation of the crucible, and "t_m" is the total duration where the crucible was translated during the experiment (which in this case is 55 h). The concentration of Si incorporated in the growing crystal (C_S) for "g" corresponding to time "t" was calculated using the equation[29]

$$C_s(g) = k_0[C_0]_t,$$

where k_0 is the equilibrium segregation coefficient of Si in Ge,

which is reported to be 5.25 by previous works.[15,18,29] The Si concentration, which is theoretically determined along the crystal given in Fig. 4(a), exhibits a trend that closely aligns with the measured Si concentration within the crystal. The variance observed between the theoretical and the measured Si distribution in the crystal suggests a lower incorporation of Si in the crystal than expected. Some of the factors that greatly influence the incorporation of Si include inhomogeneous melt composition and the dissolution rate of Si in the $\text{Si}_x\text{Ge}_{1-x}$ melt.[15,16,18] Nevertheless, the theoretical Si distribution eases the determination of pre-growth conditions to achieve the target Si concentration in the Cz-grown $\text{Si}_x\text{Ge}_{1-x}$ crystals.
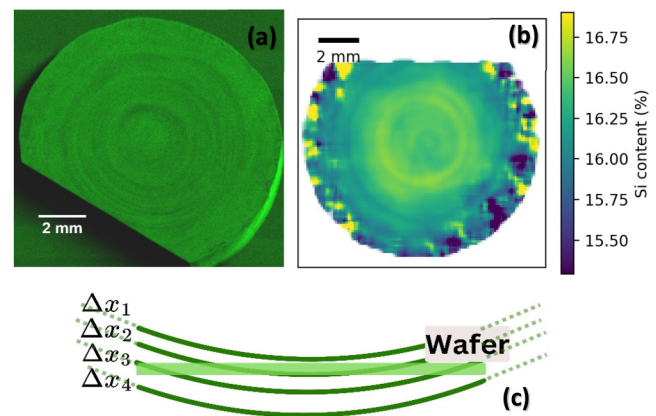
FIG. 5. (a) EDLM result of a wafer obtained from approximately 3.2% g, (b) Si distribution on the wafer shown in (a) derived from the change in the lattice parameter measured using the XRD-RCI technique, and (c) schematic of the position of the wafer shown in (a) and (b) in comparison to the crystal growth striations. Δx_1 Δx_2 Δx_3, and Δx_4 correspond to the change in Si concentration as the growth front proceeds.

04 March 2025 09:07:20

FIG. 6. (a) EDLM of the grown crystal. The solidified fractions shown in the map correspond to the region between 1% g and 4.5% g. (b) WB-XRT map obtained from an 800 μm thick sample obtained from the indicated region in the EDLM map of the grown crystal using a 040 symmetric reflection. The features in white indicate dislocation networks.

An EDLM map of the wafer, shown in Fig. 5(a), indicates the presence of several ring-like structures; similar to the growth rings of a tree. The separation between the rings is in the order of 100 μm. T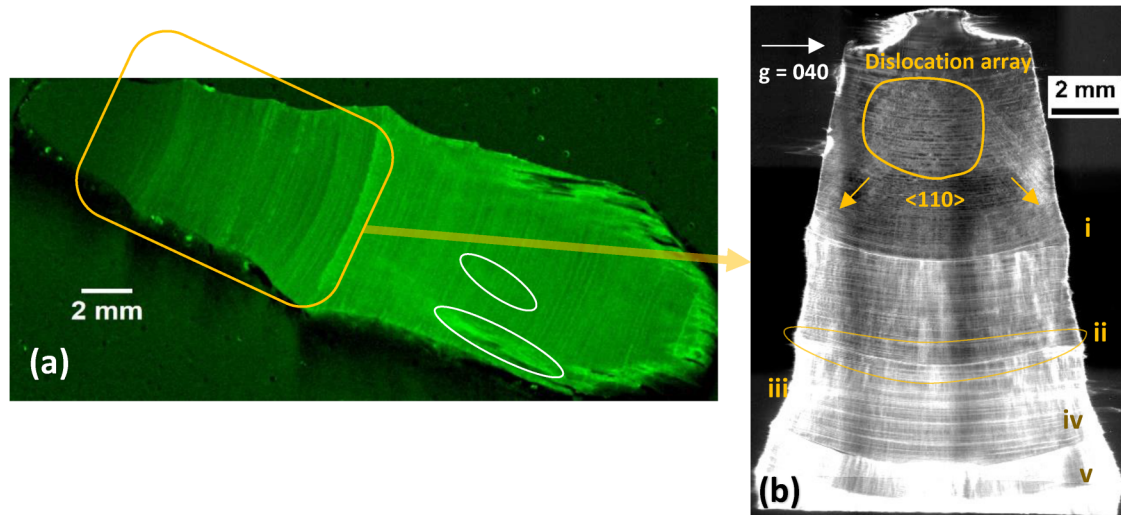hese ring structures correspond to the growth striations, a small variation in the Si concentrations as the growth front (boundary layer) advances.[15,18] These striations have the shape of the boundary layer between the crystal and the melt, which is convex. Consequently, planar wafers are expected to show ring-like Si concentration oscillation, as indicated in the schematic shown in Fig. 5(c).

RCI was employed to map the lattice parameters of the wafer, from which the Si concentration [see Fig. 5(b)] was calculated as described in the experimental section. The Si concentration measured on the single crystalline region of the wafer is >16 at. % Si. The highest Si concentrations above 16.6 at. % were measured toward the center of the wafer. Furthermore, the position of the prominent ring-like structure seen in the RCI map is in good agreement with the ring structures seen in Fig. 5(a).

The fluctuations in the Si concentration at the edges indicate abrupt changes in the lattice parameter over small distances indicating poly-crystallinity. This is mainly due to the thermal stresses at the edges of the growing crystal between the crystal and the melt.

From the results obtained, the variation of the Si concentration on the central single crystalline region of the wafer is observed to be approximately 0.4 at. %. These Si fluctuations can be compared to the cross-hatch pattern in strain-relaxed SiGe buffers, which are concentration undulations following the $\langle 110 \rangle$ directions in the (001) plane. The Si undulations of a cross-hatch in a comparable SiGe buffer are in the order of 1 at. % with modulation of around 5 μm.[30] Consequently, the Cz-SiGe material exhibits lower variation in Si concentration together with a larger spatial separation between peaks and valleys.

STRUCTURAL ANALYSIS

The investigation of crystalline defects present in the crystal is based on the EDLM, WB-XRT, and EPD techniques.

An EDLM of the longitudinal cross section of the crystal is depicted in Fig. 6(a). This measurement shows the region toward the outer parts, which show signs of small-angle grain boundaries (<5°) and areas of higher dislocation density as highlighted by white ellipses in Fig. 6(a). The bulk part of the crystals proves to be rather homogeneous except for undulations that are present due to the above-mentioned growth striations.

WB-XRT was used to image the evolution of the structure at the top part of the crystal, where the Si concentration gradually increases from 0 to 14 at. %. For this, a double-sided-polished cross section of the crystal with a thickness of 800 μm was prepared. Figure 6(b) shows the obtained x-ray topography mapping using 040 reflection.

The very top part of the crystal containing pure Ge is dislocation-free. Correspondingly, the initial dislocation network in the crystal was observed in the region containing >1 at. % Si. These dislocation arrays, marked in yellow in Fig. 6(b), correspond to an approximate dislocation density of 10^3 cm^{-2}.

The dislocation density was observed to gradually increase, proportional to the Si concentration in the crystal. Several jumps in Si concentration are marked in Fig. 6(b) by (i), (ii), (iii), (iv), and (v). With each concentration jump, the dislocation density increases significantly, until individual dislocation cannot be resolved anymore. Furthermore, the curvature of the melt–crystal interface is seen to be changing with each jump. This could be due to the excess Si in front of the crystal–melt interface resulting in a slightly higher melting point than that of the growing crystal. Such a growth regime is known to introduce dislocations and cellular
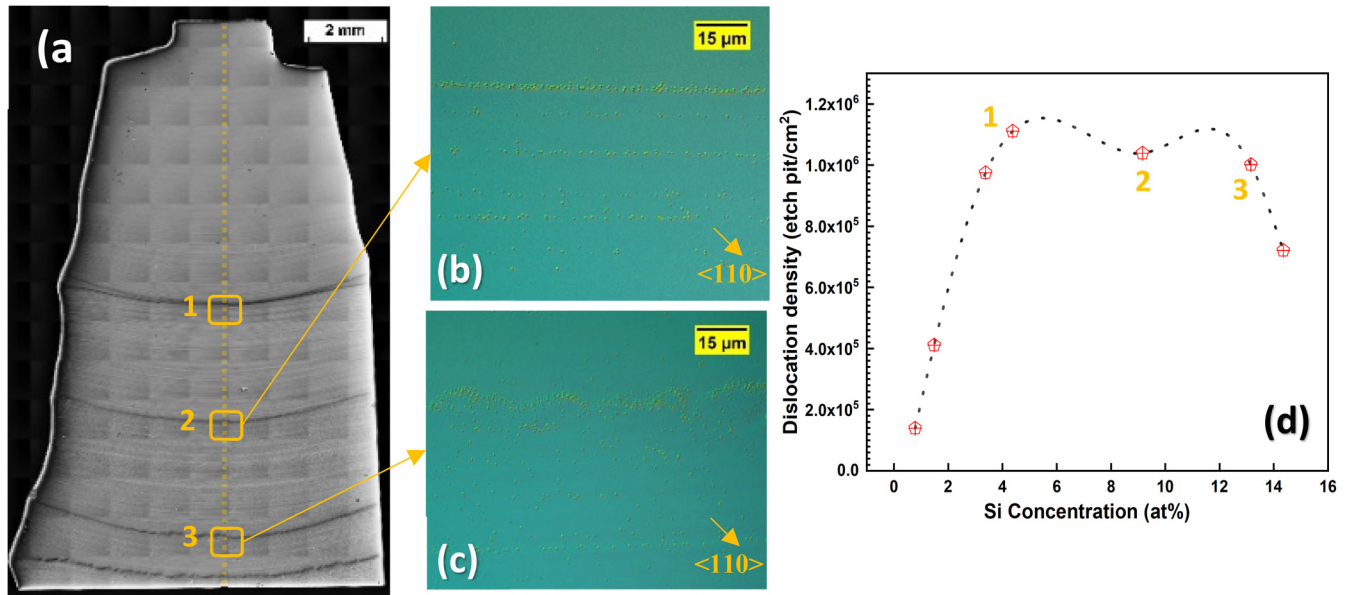
04 March 2025 09:07:20

FIG. 7. Etch pit density measurements: (a) position of the dislocations quantified along the center of the etched longitudinal cut, (b) magnified image of position 2, (c) magnified image of position 3 showing the sudden shift to a multi-crystalline regime and then back to single crystalline, and (d) graph comparing the quantified dislocation density vs the Si concentration along the length of the longitudinal sample shown in (a).

structures finally leading to the introduction of small-angle grain boundaries in the crystal.[31,32]

The dislocation density in the crystal was further investigated using dislocation-selective etching. For this, two samples were investigated; a longitudinal cut sample cross section along the growth direction [same as the one used for WB-XRT and EDLM in Fig. 6(b)] and a wafer obtained [same as the one used for EDLM and RCI as shown in Figs. 5(a) and 5(b)].

The etch pits were quantified within the central region of the longitudinal cross-sectional cut, as depicted in Fig. 7(a). Detailed microscopy images with a differential interference contrast of two selected regions exhibiting several etch pits with diameters ranging between 1 and $5\,\mu$m are shown in Figs. 7(b) and 7(c). The majority of these etch pits were seen to be aligned along the melt–crystal interface, which indicates that the dislocations were introduced to accommodate the misfit resulting from the abrupt decrease in lattice constant with increasing Si concentration. Furthermore, the etch pit counts indicated by the red open hexagon shown in Fig. 7(d) represent the dislocation densities at Si "jumps" along the longitudinal cross section of the crystal. The etch pit density along the cross section follows a trend as depicted by the dotted line in Fig. 7(d).

The average distance between these lines of arranged etch pits is the order of μm. This can be understood (and even quantified) by the relaxation mechanism described by People and Bean[33] as well as by Matthews and Blakeslee.[34] The relaxation mechanism was developed for epitaxial thin films, but its adaption to a growing bulk crystal is sketched in Fig. 8(a). The continuous lines along the crystal cross section shown in the schematic represent the pre-existing dislocations in the crystal. The regions a_1, a_2, and a_3

represent solidified melt fractions with slightly different lattice constants due to different Si concentrations incorporated along the growing Si_xGe_{1-x} crystal. Furthermore, these regions (a1, a2, and a3) are separated in the crystal by a Si "jump."

Here, the crystalline structure of subsequent crystallizing melt fractions with varying Si concentrations is considered analogous to that of an epitaxially grown layer with a mismatch in lattice constant. This mismatch typically arises due to abrupt changes in the Si concentration during the growth process. Initially, the growing crystal with increasing Si concentration contains the extended pre-existing dislocations. The force acting on these dislocations is proportional to the dislocation length assuming a constant lattice mismatch between the layers. When the crystal reaches a certain critical thickness (and consequently a certain length of dislocations in this grown crystal) following a Si jump, the force becomes sufficient to generate new dislocation segments [indicated by the dotted arrows in Fig. 8(a)]. These misfit dislocation segments lie within the regions close to the Si concentration jumps and represent the primary dislocations causing etch pits observed in Figs. 7(a)–7(c).

The critical thickness h_c for relaxation and corresponding misfit dislocation formation can be described as

$$h_c \approx \frac{b}{4\pi f(1+\nu)}\left[\ln\left(\frac{h_c}{b}\right)+1\right],$$

where f is the lattice mismatch, ν is the Poisson ratio (0.27 for Ge), and b is the Burgers vector (0.4 nm for pure Ge). The misfit is related to the small Si jumps during growth and is typically less
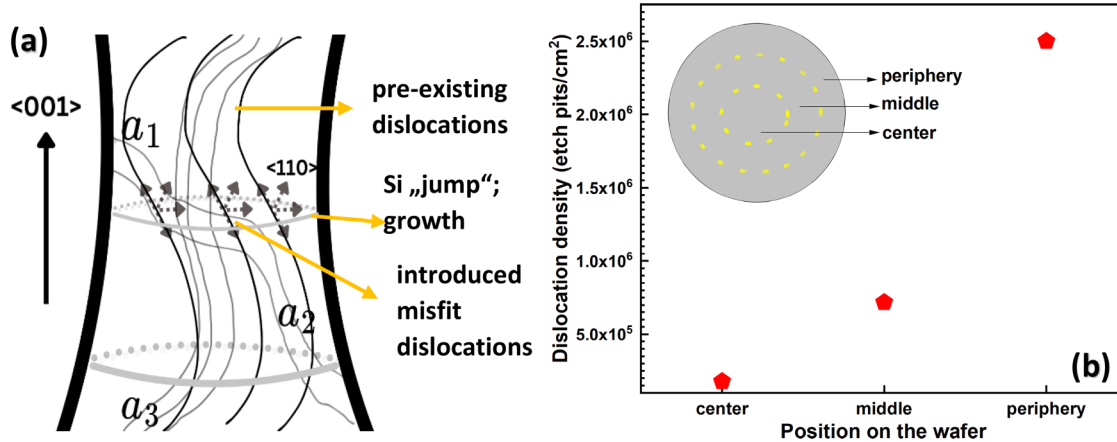
FIG. 8. (a) Sketch of the assumed dislocation generation mechanism in the grown SiGe crystal; a_1, a_2, and a_3 indicate the regions with slightly different lattice constants corresponding to solidified melt fractions after a Si "jump." The continuous lines indicate the pre-existing dislocations in the crystal. The dotted lines at the interface between regions a_1 and a_2 represent the introduced misfit dislocations and (b) dislocation density quantified on the wafer taken from about 3.2% g. The wafer surface was divided into three regions, center, middle, and periphery, which is indicated by the image in the plot.

than 1 at. %, as identified by XRF in Fig. 4(b). This results in a misfit in the order of $<10^{-4}$, based on Vegard's law and a lattice constant of Ge and Si of 0.566 and 0.543 nm, respectively. The corresponding critical thickness is then in the order of μm ($>2\,\mu$m for the values mentioned above), in approximate agreement with the observed Si concentration profile and dislocation distribution.

Furthermore, the dislocations terminating on the surface of the wafer (same as the one used for EDLM analysis) were revealed using the EPD method. The resulting etch pits were counted in three different regions, namely, center, middle, and periphery as shown in Fig. 8(b). The dislocation density measured in the center of the wafer is approximately $2 \times 10^5\,\mathrm{cm}^{-2}$. An increase in dislocation density is observed toward the edge of the wafer. This higher dislocation density in the peripheral regions can be primarily attributed to thermal stress present at the interface between the growing crystal and the Si_xGe_{1-x} melt.

DISCUSSION AND CONCLUSION

Adopting a continuous feeding method to incorporate Si[15] into the Ge melt is effective to grow Si_xGe_{1-x} single crystals containing up to 18 at. % Si. Previous works have reported a polycrystalline growth regime of Si_xGe_{1-x} single crystals with $x < 0.15$ and $x > 0.85$.[15,16,18,35] The polycrystalline formation was observed below the critical velocities determined by Tiller's criteria.[18] These results suggest the inhomogeneous dissolution of Si in the Ge melt is detrimental to the crystalline structure of the grown SiGe crystal. In this work, dislocation densities $<10^5\,\mathrm{cm}^{-2}$ were achieved in regions with Si concentrations greater than 18 at. %. Furthermore, the high-purity feed material used for the Cz growth ensured a high purity of the produced crystal.

The pulling rates and the gradual increments in crystallization temperature were carefully controlled, closely monitoring the Si "jumps" during the crystal growth process. Regions of the crystal where a spontaneous increase in the Si concentration (Si "jumps") are

observed to be the main sources of dislocations in the crystal are in good agreement with previously done studies.[15,18] Hence, efforts toward achieving a more gradual and continuous increase in the Si concentration without concentration jumps in the crystal is a promising approach to reduce the introduced dislocations. Previous studies suggest that higher Si concentrations lead to an increase in introduced dislocations within the crystal.[15,18,36] However, the current results suggest that a lower dislocation density ($<10^5\,\mathrm{cm}^{-2}$) can be achieved with a homogenous dissolution of Si. One way of achieving better control could be to set smaller dip rates of the Si rods, which enables better control over Si integration into the Ge melt. The spontaneous dissolution of significant amounts of Si into the Ge melt raises the crystallization temperature, inducing constitutional supercooling. Precisely controlling this phenomenon can be challenging due to the rapid incorporation of Si into the crystal, driven by the large segregation coefficient of Si in Ge ($\gg 1$). Consequently, the subsequent solidified melt requires a lower crystallization temperature, heightening the risk of crystal back-melting and potentially jeopardizing the success of the growth experiment. Furthermore, the application of external forces could enhance the melt convection resulting in a more homogeneous melt and better control of the solid–liquid interface. The current findings suggest the potential for achieving higher Si concentrations in Ge bulk crystals. Further experiments are required to refine the crystal growth parameters, including the incremental temperature gradient, pulling rate, number of Si rods, and, most importantly, develop an accurate model for Si dissolution in the Ge melt. Additionally, fabricating the Ge quantum well heterostructure using $Si_{1-x}Ge_x$ substrates from regions with a high Si concentration (>18 at. %) and low dislocation density ($<10^6\,\mathrm{cm}^{-2}$) in the bulk crystal would facilitate validation of the approach.

04 March 2025 09:07:20

AUTHOR DECLARATIONS

Conflict of Interest

The authors have no conflicts to disclose.

Author Contributions

Aravind N. Subramanian: Data curation (equal); Formal analysis (equal); Investigation (equal); Methodology (equal); Validation (equal); Visualization (equal); Writing – original draft (lead); Writing – review & editing (equal). **Carsten Richter:** Formal analysis (equal); Investigation (equal); Methodology (equal); Visualization (equal); Writing – review & editing (equal). **Alexander Gybin:** Formal analysis (equal); Investigation (equal); Methodology (equal). **Merve P. Kabukcuoglu:** Formal analysis (equal); Investigation (equal); Methodology (equal); Visualization (equal); Writing – review & editing (equal). **Elias Hamann:** Formal analysis (equal); Funding acquisition (equal); Investigation (equal); Visualization (equal); Writing – review & editing (equal). **Marcus Zuber:** Formal analysis (equal); Investigation (equal); Methodology (equal); Visualization (equal); Writing – review & editing (equal). **Maximilian Oezkent:** Data curation (equal); Formal analysis (equal); Investigation (equal); Methodology (equal); Validation (equal); Writing – review & editing (equal). **Christo Guguschev:** Data curation (equal); Formal analysis (equal); Investigation (equal); Methodology (equal); Validation (equal); Visualization (equal); Writing – review & editing (equal). **Uta Juda:** Formal analysis (equal); Investigation (equal); Methodology (equal); Writing – review & editing (equal). **Thomas Schroeder:** Conceptualization (equal); Funding acquisition (equal); Resources (equal); Validation (equal); Writing – review & editing (equal). **Nikolay V. Abrosimov:** Conceptualization (equal); Investigation (equal); Validation (equal); Writing – review & editing (equal). **R. Radhakrishnan Sumathi:** Formal analysis (equal); Resources (equal); Validation (equal); Writing – review & editing (equal). **Kevin-P. Gradwohl:** Conceptualization (equal); Data curation (equal); Formal analysis (equal); Investigation (equal); Methodology (equal); Project administration (equal); Supervision (equal); Validation (equal); Visualization (equal); Writing – original draft (equal); Writing – review & editing (equal).

DATA AVAILABILITY

The data that support the findings of this study are available from the corresponding author upon reasonable request.

REFERENCES

[1]G. Scappucci, C. Kloeffel, F. A. Zwanenburg, D. Loss, M. Myronov, J.-J. Zhang, S. De Franceschi, G. Katsaros, and M. Veldhorst, "The germanium quantum information route," Nat. Rev. Mater. **6**, 926 (2020).

[2]N. W. Hendrickx, L. Massai, M. Mergenthaler, F. J. Schupp, S. Paredes, S. W. Bedell, G. Salis, and A. Fuhrer, "Sweet-spot operation of a germanium hole spin qubit with highly anisotropic noise sensitivity," Nat. Mater. **23**, 920 (2024).

[3]N. W. Hendrickx, W. I. L. Lawrie, L. Petit, A. Sammak, G. Scappucci, and M. Veldhorst, "A single-hole spin qubit," Nat. Commun. **11**, 3478 (2020).

[4]N. W. Hendrickx, W. I. L. Lawrie, M. Russ, F. van Riggelen, S. L. de Snoo, R. N. Schouten, A. Sammak, G. Scappucci, and M. Veldhorst, "A four-qubit germanium quantum processor," Nature **591**, 580 (2021).

[5]C.-A. Wang *et al.*, "Operating semiconductor quantum processors with hopping spins," Science **385**, 447 (2024).

[6]W. I. L. Lawrie *et al.*, "Quantum dot arrays in silicon and germanium," Appl. Phys. Lett. **116**(8), 080501 (2020).

[7]L. E. A. Stehouwer, A. Tosato, D. Degli Esposti, D. Costa, M. Veldhorst, A. Sammak, and G. Scappucci, "Germanium wafers for strained quantum wells with low disorder," Appl. Phys. Lett. **123**, 092101 (2023).

[8]L. E. Stehouwer, C. X. Yu, B. van Straaten, A. Tosato, V. John, D. D. Esposti, A. Elsayed, D. Costa, S. D. Oosterhout, N. W. Hendrickx, and M. Veldhorst, "Exploiting epitaxial strained germanium for scaling low noise spin qubits at the micron-scale," arXiv:2411.11526 (2024).

[9]L. Becker, "Controlling the relaxation mechanism of low strain Si$_{1-x}$Ge$_x$/Si (001) layers and reducing the threading dislocation density by providing a preexisting dislocation source," J. Appl. Phys. **128**, 215305 (2020).

[10]C. Corley-Wiciak *et al.*, "Nanoscale mapping of the 3D strain tensor in a germanium quantum well hosting a functional spin qubit device," ACS Appl. Mater. Interfaces **15**, 3119 (2023).

[11]F. Rovaris *et al.*, "Dynamics of crosshatch patterns in heteroepitaxy," Phys. Rev. B **100**, 085307 (2019).

[12]M. H. Zoellner *et al.*, "Imaging structure and composition homogeneity of 300 mm SiGe virtual substrates for advanced CMOS applications by scanning X-ray diffraction microscopy," ACS Appl. Mater. Interfaces **7**, 9031 (2015).

[13]W. C. Dash, "Growth of silicon crystals free from dislocations," J. Appl. Phys. **30**, 459 (1959).

[14]A. Bhat, O. Elleuch, X. Cui, Y. Guan, S. A. Scott, T. F. Kuech, and M. G. Lagally, "High-Ge-content SiGe alloy single crystals using the nanomembrane platform," ACS Appl. Mater. Interfaces **12**, 20859 (2020).

[15]N. V. Abrosimov, S. N. Rossolenko, W. Thieme, A. Gerhardt, and W. Schröder, "Czochralski growth of Si- and Ge-rich SiGe single crystals," J. Cryst. Growth **174**, 182 (1997).

[16]I. Yonenaga, "Growth and fundamental properties of SiGe bulk crystals," J. Cryst. Growth **275**, 91 (2005).

[17]I. Yonenaga, T. Taishi, Y. Ohno, and Y. Tokumoto, "Cellular structures in Czochralski-grown SiGe bulk crystal," J. Cryst. Growth **312**, 1065 (2010).

[18]I. Yonenaga, "Czochralski growth of GeSi bulk alloy crystals," J. Cryst. Growth **198–199**, 404 (1999).

[19]J. Sherman, "The theoretical derivation of fluorescent X-ray intensities from mixtures," Spectrochim. Acta **7**, 283 (1955).

[20]C. Guguschev, R. Tagle, U. Juda, and A. Kwasniewski, "Microstructural investigations of SrTiO$_3$ single crystals and polysilicon using a powerful new X-ray diffraction surface mapping technique," J. Appl. Crystallogr. **48**, 1883 (2015).

[21]C. Guguschev, C. Richter, M. Brützam, K. Dadzis, C. Hirschle, T. M. Gesing, M. Schulze, A. Kwasniewski, J. Schreuer, and D. G. Schlom, "Revisiting the growth of large (Mg,Zr):SrGa$_{12}$O$_{19}$ single crystals: Core formation and its impact on structural homogeneity revealed by correlative X-ray imaging," Cryst. Growth Des. **22**, 2557 (2022).

[22]J. P. Dismukes, L. Ekstrom, and R. J. Paff, "Lattice parameter and density in germanium-silicon alloys," J. Phys. Chem. **68**, 3021 (1964).

[23]A. N. Danilewsky *et al.*, "Real-time X-ray diffraction imaging for semiconductor wafer metrology and high temperature *in situ* experiments," Phys. Status Solidi A **208**, 2499 (2011).

[24]F. Secco d' Aragona, "Dislocation etch for (100) planes in silicon," J. Electrochem. Soc. **119**, 948 (1972).

[25]R. W. Olesinski and G. J. Abbaschian, "The Ge−Si (germanium-silicon) system," Bull. Alloy Phase Diagrams **5**, 180 (1984).

04 March 2025 09:07:20

[26]O. V. Smirnova, V. V. Kalaev, Y. N. Makarov, N. V. Abrosimov, and H. Riemann, "Simulation of heat transfer and melt flow in Czochralski growth of Si1−xGex crystals," J. Cryst. Growth **266**, 74 (2004).

[27]W. Miller, N. Abrosimov, I. Rasin, and D. Borissova, "Cellular growth of single crystals," J. Cryst. Growth **310**, 1405 (2008).

[28]L. I. Khirunenko, O. O. Kobzar, Y. V. Pomozov, M. G. Sosnin, M. O. Tripachko, N. V. Abrosimov, and H. Riemann, "Interstitial-related reactions in silicon doped with isovalent impurities," Physica B **340–342**, 546 (2003).

[29]W. G. Pfann, "Principles of zone-melting," J. Miner. Met. Mater. Soc. (TMS) **4**, 747 (1952).

[30]G. Capellini, M. De Seta, Y. Busby, M. Pea, F. Evangelisti, G. Nicotra, C. Spinella, M. Nardone, and C. Ferrari, "Strain relaxation in high Ge content SiGe layers deposited on Si," J. Appl. Phys. **107**, 063504 (2010).

[31]P. Rudolph, "Fundamentals and engineering of defects," Prog. Cryst. Growth Charact. Mater. **62**, 89–110 (2016).

[32]A. Subramanian *et al.*, "Investigation of doping processes to achieve highly doped Czochralski germanium ingots," J. Electron. Mater. **52**, 5178 (2023).

[33]R. People and J. C. Bean, "Calculation of critical layer thickness versus lattice mismatch for Ge_xSi_{1-x}/Si strained-layer heterostructures," Appl. Phys. Lett. **47**, 322 (1985).

[34]J. W. Matthews and A. E. Blakeslee, "Defects in epitaxial multilayers," J. Cryst. Growth **27**, 118 (1974).

[35]J. Schilz and V. N. Romanenko, "Bulk growth of silicon-germanium solid solutions," J. Mater. Sci. Mater. Electron. **6**, 265 (1995).

[36]D. Borisova, N. V. Abrosimov, K. Shcherbachev, V. Klemm, G. Schreiber, D. Heger, U. Juda, V. Bublik, and H. Oettel, "Evolution of real structure in Ge-Si mosaic crystals," Cryst. Res. Technol. **51**, 742 (2016).

04 March 2025 09:07:20